RSC Advances

ROYAL SOCIETY OF CHEMISTRY

www.rsc.org/advances

The long persistent luminescence properties of phosphors: Li_2ZnGeO_4 and $Li_2ZnGeO_4:Mn^{2+}$

Yahong Jin, Yihua Hu*, He Duan, Li Chen, Xiaojuan Wang

School of Physics and Optoelectronic Engineering, Guangdong University of Technology, WaiHuan Xi Road, No.100, Guangzhou 510006, PR China

The blue emitting long persistent phosphor (LPP) Li_2ZnGeO_4 and green emitting LPP $Li_2ZnGeO_4:Mn^{2+}$ were newly prepared by a high temperature solid-state reaction method. The blue and green afterglow with duration of 5 and 8 h were confirmed to the origination from host emission and d–d transitions of Mn^{2+} ions, respectively. The density of traps with suitable depth was significantly increased with the incorporation of Mn^{2+} ions. The energy transfer from host emission to Mn^{2+} ions was observed. The motion of charge carriers and a possible LAG mechanism based on a tentative model were illuminated and discussed in detail.

***Corresponding author.**
Tel: +86 20 39322262;
Fax: +86 20 39322265.
Email address: huyh@gdut.edu.cn (Y.Hu)

Introduction

Long persistent phosphor is a kind of energy absorbing, storing and releasing material. Under the excitation of sunlight or other artificial light source, it can absorb and store energy and then release the energy gradually for several seconds to hours in the form of visible light after the stoppage of excitation source at room temperature [1-3]. LPPs can find applications in many fields such as security illumination, decoration, storage media, detection of high energy rays and fiber-optic thermometers and in vivo bio-imaging [4] due to the environmentally friendly, economically sustainable and unique properties.

Since the report of $SrAl_2O_4:Eu^{2+}$, Dy^{3+} by Matsuzawa et al. in 1996 [5], many researchers have paid much attention on the development of divalent europium doped LPPs and a large number of LPPs that Eu^{2+}-doped in various matrices have been discovered [6]. During the past decades, the number of publications on non-Eu^{2+}-doped (mainly includes trivalent rare-earth ions and transition metal ions) LPPs have also seen a steady increase. However, compared to the Eu^{2+}-doped LPPs, the luminance and duration of the present non-Eu^{2+}-doped LPPs are still poor. The lack of excellent non-Eu^{2+}-doped LPPs is striking. Furthermore, to explain the occurrence of long afterglow (LAG) and solve the unrevealed problems, several different kinds of models on LAG mechanism have been proposed such as Dorenbos [7] and Holsa [8]. Unfortunately, there are still many unknown details such as the nature of traps and the interaction between traps which are critical to explore and design the desired LPPs though most authors have reached an agreement on the

general idea that charge carriers are trapped by long-lived traps inside the band gap. In order to better understand the LAG generation process and pave the way for the further development of LPPs avoiding some unnecessary detours, it is urgent to unravel these mysteries. Thus, it is necessary to in search for various new kinds of LPPs with different lattice host and activators to unravel and complete the mechanism behind the LAG.

Recently, Mn^{2+}-doped germanates such as Zn_2GeO_4 and Li_2ZnGeO_4 have attracted much more interest due to the excellent performance and potential practical application in field-emission displays [9, 10]. Divalent manganese ion has a d^5 electron configuration with a broad emission band varying from deep green to far red depending on the strong ligand of the $^4T_1(^4G)$ state and the emission is ascribed to the parity-forbidden d-d transition from the lowest excited level $^4T_1(4G)$ to the ground state $^6A_1(6S)$ [11]. As an important activator, Mn^{2+} ion has been extensively employed in a large number of important phosphors. But, up to now, few studies about Mn^{2+} solely doped LPPs have been reported, for examples, $CaZnGe_2O_6:Mn^{2+}$ (red) [12], $CdSiO_3:Mn^{2+}$ (orange) [13] and Zn_2GeO_4: Mn^{2+} (green) [14]. These motivated us to predict that Li_2ZnGeO_4 may have the potential to serve as a new host material for Mn^{2+} with LAG emission.

Therefore, in our present work, Li_2ZnGeO_4 and Mn^{2+} were selected as host and activator, respectively. Phosphors of un-doped Li_2ZnGeO_4 and Mn^{2+}-doped Li_2ZnGeO_4 were synthesized successfully by high temperature solid state method. Accordingly, a green emitting LPP $Li_2ZnGeO_4:Mn^{2+}$ with excellent LAG properties

was obtained, just as we anticipated. To our surprise, the phenomenon of blue LAG originating from un-doped Li_2ZnGeO_4 was also observed. According to the photoluminescence, afterglow, decay curves and TL glow curves, the traps in lattice and the generation mechanism of LAG were discussed in detail on basis of a schematic.

Experiments

Sample Synthesis

Powder samples of Mn^{2+}-doped Li_2ZnGeO_4 (LZGO) phosphors were prepared via a conventional high temperature solid state reaction method. The starting materials used in the preparation were Li_2CO_3 (AR), ZnO (AR), $MnCO_3$ (AR) and GeO_2 (99.99%). The stoichiometric amounts of raw materials were weighed out according to the nominal compositions of $Li_2Zn_{1-t}GeO_4$:tMn^{2+} (t=0, 0.0025, 0.005, 0.01, 0.015, and 0.02). Then the powders were mixed and homogenized thoroughly for 40 min in an agate mortar. Next, the mixtures were transferred into alumina crucibles and calcined at 1200 ℃ for 4 h in a tube furnace in air atmosphere. After cooling down to room temperature naturally, all as-synthesized samples were ground again to fine powders in an agate mortar.

Measurements and Characterization

The phase identification of samples LZGO:tMn (t=0, 0.0025, 0.01 and 0.02) were carried out by a XD-2 powder diffractometer (Beijing PGENERAL) using Cu Kα irradiation (λ=1.5406 Å) at 36 kV tube voltage and 20 mA tube current with a scanning step of 0.02° in the 2θ range from 10° to 70°. In order to carry out a

whole-powder-pattern profile fitting, the XRD data of all as-prepared samples were also collected in the 2θ range from 10° to 110° with intervals of 0.02° and a pace time of 2 s per step. These data diffraction data were collected on aRigaku X-ray diffractometer D/Max-2400 with a power of 40 kV at 140 mA, employing Cu K*a* radiation by using a graphite monochromator. The divergence, scattering, and receiving slit were set at 18, 18 and 0.3 mm, respectively. Structure refinements of all obtained samples were performed by a Fullprof program [15] using a whole-powder-pattern profile fitting procedure. The excitation and emission spectra were measured using a Hitachi F-7000 Fluorescence Spectrophotometer equipped with a Xe lamp (150 W) as excitation source. Both the slits of excitation and emission were set to be 2.5 nm. The scanning rate was 1200 nm/min under 400V working voltage. Suitable filters were used to avoid the appearance of diffraction peaks. The afterglow spectra were also obtained by the same Hitachi F-7000 Fluorescence Spectrophotometer. The UV excitation source was switching off after the samples were irradiated by 254 nm for 3 min and the afterglow spectra were recorded immediately. Afterglow decay curves were recorded immediately after the samples being irradiated by 254 nm for 2 min with a GFZF-2A single-photon counter system. A FJ427A1 thermoluminescent dosimeter (CNNC Beijing Nuclear Instrument Factory) was utilized to collect the TL curves from room temperature to 250 ℃ with a heating rate of 1 □/S. Prior to the TL measurements, each sample was first exposed to a 254 nm UV radiation lamp (60 W) for 1 min and then put in dark waiting for 2 min. To ensure the validity of comparison, the amount of each sample for afterglow decay and

TL measurements was kept as a constant. All the measurements were performed at room temperature except for the TL curves.

Results and discussion

Phase identification

Fig. 1 shows X-ray powder diffraction patterns of some selective samples LZGO: tMn^{2+} (t=0, 0.0025, 0.01 and 0.02) and standard card of compound Li_2ZnGeO_4. It can be clearly seen that all diffraction peaks are matched well with the standard data of Li_2ZnGeO_4 (JCPDS No. 38-1082) indicating the high purity and crystalline of the samples in this work. Fig. 2(a)-(f) exhibit the experimental, fitted and difference results of the XRD refinements using Rietveld refinement for powder XRD data of LZGO:tMn (t=0, 0.0025, 0.005, 0.01, 0.015 and 0.02 respectively) at room temperature. The corresponding structure parameters are listed in Table 1(a). Based on it, the structure of Li_2ZnGeO_4 can be assigned to the monoclinic crystal system with space group $P2_1/n$. The reliability parameters of refinements for all as-obtained samples are listed in Table 1(b). The LZGO host lattice is built up by GeO_4 tetrahedra, which are linked together by LiO_4 and $Zn(Mn)O_4$ tetrahedra [16, 17]. No extra phase can be observed inferring that Mn^{2+} ions have been completely dissolved into the LZGO host lattice by substitution for Zn sites and such a small amount of Mn^{2+} ions doping does not have significant influence on the crystal structure of host.

Photoluminescence properties

The excitation and emission spectra of LZGO and LZGO:Mn^{2+} in UV-vis range are shown in Fig. 3. For non-doped sample LZGO, a broad excitation band from 200 to

280 nm with a maximum at 245 nm can be observed when monitoring emission at 396 nm. Under excitation by 245 nm, it shows a broad emission band between 300 and 600 nm with a peak at ~396 nm. The blue emission can be attributed to the recombination of donors ($V_O^{\bullet\bullet}$ and $Zn_i^{\bullet}$) and acceptors ($V_{Ge}^{''''}$ and $V_{Zn}^{''}$) which are associated with native defects [18, 19]. Compared to the results by Shang et al. [10], there is slight wavelength shift of excitation and emission. In this paper, some more details of photoluminescence are observed. For Mn^{2+} doped LZGO samples, when monitoring emission at 530 nm, a broad strong excitation band with a maximum at 266 nm which is assigned to the charge-transfer transition in Mn^{2+} ions [20] and several weak sharp peaks which are attributed to the transitions of $^6A_1(^6S)$ to $^4E(^4D)$, $^4T_2$ (^4D), $^4T_2$ (^4G) and $^4T_1$ (^4G) (seen in Fig. 3(b)) can be observed. Upon excitation by 266 nm, two broad separated corresponding emission bands are observed. One emission band in the range from 300 to 500 nm with a peak at ~367 nm (seen in Fig. 3(c)) is related to the emission of LZGO host. Compared to the emission of un-doped LZGO, it shows significant blue shift, which may be resulted from the distortion distribution of donors and acceptors as the incorporation of Mn^{2+} ions. Another emission band between 480 and 600 nm is attributed to $^4T_1$-$^6A_1$ forbidden transition of the Mn^{2+} ions. Moreover, it is notable that the emission spectrum of LZGO host covers the excitation of Mn^{2+}. So it is reasonable to conclude that the energy transfers from host to Mn^{2+} ions.

After the excitation of 254 nm UV lamp is switched off, an unexpected result of the present work is that the blue and green LAG in un-doped and Mn^{2+} doped LZGO can

be clearly observed for more than 5 and 8 h by the naked eyes in the dark room, respectively. The photos of non-doped and Mn^{2+} doped LZGO before, under and after irradiation by UV light can be seen in the inset of Fig. 4. The afterglow spectra of all obtained samples were recorded as shown in Fig. 4. The shape and position of spectra are almost the same as emission spectra (in Fig. 3). The un-doped LZGO only shows blue LAG emission. The Mn^{2+} doped LZGO mainly shows green LAG emission and the intensity decrease with the rising of Mn^{2+} contents. The optimal Mn^{2+} concentration for afterglow is not observed though the content of Mn^{2+} is already as small as t=0.0025. In addition, the extremely weak LAG emission of LZGO: Mn^{2+} in the range of 300-450 nm which is related to the host emission is also observed. The emissions decrease and disappear with the increase of Mn^{2+} contents, which confirms the ET from host to Mn^{2+}. The significant blue shift of emission band is attributed to the influence of donors and acceptors by the incorporation of Mn^{2+} ions.

Decay of afterglow

In order to study the afterglow decay behavior in more detail and compare the decay rates between LZGO samples with different Mn^{2+} doping contents, the decay curves in the time range of 0-1000 s of all as-obtained samples are collected and shown in Fig. 5. They can be well fitted and analyzed with a bi-exponential Eq. (1) as follows:

$$I = I_1 \exp(-\frac{t}{\tau_1}) + I_2 \exp(-\frac{t}{\tau_2}) \quad (1)$$

where I represents intensity; I_1 and I_2 are constants; τ_1 and τ_2 are decay times for the exponential component, they determine the rapid and slow decay processes, respectively; t is time. The fitting results of all decay curves are listed in Table 2.

Apparently, the fitting results indicate that there are two decay processes are involved in LAG decay process including a rapid decay process at first and then a slow decay process. For Mn^{2+}-doped LZGO samples, the values of τ_1 and τ_2 present continuous decreasing trends along with the increase of Mn^{2+} ions concentration. Thus, it can be concluded that LZGO: 0.0025Mn shows the best LAG performance in our work.

Thermoluminescence analysis

It is well known that LAG is primarily attributed to trapping and de-trapping of charge carriers which are captured by various traps. The suitable trap depth and high trap density play crucial roles in the generation of super LAG performance. Generally, TL curve studies can provide vital information about nature of the traps and the trap levels [21, 22]. In order to characterize the traps, TL measurements were carried out on each sample. As exhibited in Fig. 6, un-doped LZGO shows an asymmetry broad TL band between 32 and 150 °C with the peak predominating at ～65 °C. For Mn^{2+} doped LZGO samples, a predominate band centered at ～65 °C and a relatively weak band at ～126 °C are observed. It is commonly considered that the lower and higher temperature of the TL bands is related to the shallower and deeper traps, respectively [23]. The suitable TL peak is situated slightly above room temperature (50-120 °C) for the excellent LAG performance [24, 25]. Therefore, the TL band centered at ～65 °C may be responsible for the blue and green LAG. Evidently, the incorporation of a slight amount of Mn^{2+} ions largely promotes the generation of traps at ～65 °C as well as the creation of new deeper traps at ～126 °C. The equivalent substitution of

Zn^{2+} by Mn^{2+} creates isoelectronic traps such as $V_{Zn}^{''}$. The TL intensities for Mn^{2+}-doped samples corresponding to 65 °C decrease continuously with the rising of Mn^{2+} doping concentration. Since that the trap density is approximately proportional to the integral intensity of TL band, the traps of sample LZGO:0.0025Mn^{2+} possess the biggest capacity to capture carriers. Undoubtedly, Mn^{2+}-doped LZGO LPP shows the best LAG performance in the case of very small Mn^{2+} doping concentration.

The mechanism of the persistent luminescence

In order to explore the motion of charge carriers and interpret the generation process of LAG emission in LZGO and LZGO:Mn clearly, a schematic of phosphorescence mechanism based on the above analyses is illustrated as Fig. 7. Under UV excitation, electrons are excited to conduction band (CB) and holes are generated in valence band (VB) in un-doped LZGO host. Some excited electrons move through CB (①) and some holes move through VB freely (②) to the native defects. Then the recombination of electrons and holes (③) resulting in the generation of host emission. However, other excited electrons and holes also can be captured by the electron and hole traps, respectively (⑦). Under the activation of thermal motion, these trapped charge carriers (electrons and holes) can escape from their respective traps to CB and VB with a slow rate and move to the native defects (⑧) leading to the process ③, which creates the blue LAG from the host. When Mn^{2+} ion is doped into the host lattice, on the one hand, those unbound excited electrons mentioned above will move around in VB jumping to the excited energy level $^4E(^4D)$ of Mn^{2+} (④) and holes have the motion via VB to the ground state of Mn^{2+} (⑤). These excited electrons in higher

energy level will transfer to the lower levels and finally to $^4T_1(^4G)$ with non-radiative transitions. Afterwards, they will jump to ground state and combines with holes accompanying with the emission from Mn^{2+} (⑥). Meanwhile, the energy from host emission (③) will transfer to the excited energy levels of Mn^{2+}. On the other hand, those gradually released electrons and holes from traps also can transfer to the excited energy level and ground state of Mn^{2+}, respectively (⑨). The same process of charge carriers motion as the intrinsic emission of Mn^{2+} (⑥) occurs with a delay time, which causes the blue LAG phenomenon from Mn^{2+} ion. Similarly, there is a great chance of energy transfer from the LAG emission to Mn^{2+} ions at the same time. Thus, the emission and LAG are largely weakened by the incorporation of Mn^{2+} ions.

Conclusions

The un-doped blue emitting long persistent phosphor Li_2ZnGeO_4 and green emitting long persistent phosphor Li_2ZnGeO_4:Mn^{2+} with excellent afterglow performance were designed, prepared and characterized. The blue and green afterglow emissions originate from the host and Mn^{2+} emission. The duration of them can persist 5 and 8 h, respectively. The energy transfer from host to Mn^{2+} ions was confirmed. A possible afterglow mechanism was proposed and the generation processes of LAG were illustrated in detail. The two brand new LPPs may have great potential application in many important fields.

Acknowledgments

The authors acknowledge the financial support from the National Natural Science Foundation of China (No. 21271049).

References

1. W. Zeng, Y. H. Wang, S. C. Han, W. B. Chen, G. Li, Y. Z. Wang, Y. Wen, J. Mater. Chem. C, 2013, **1**, 3004.

2. Y. Q. Li, Y. H. Wang, Y. Gong, X. H. Xu, M. J. Zhou, Opt. Express, 2010, **18**, 24853.

3. Y. H. Jin, Y. H.Hu, L. Chen, X. J. Wang, G. F. Ju, Z. F. Mou, J. Am. Ceram. Soc., 2013, **96**, 3821.

4. S. X. Lian, Y. Qi, C. Y. Rong, L. P. Yu, A. L. Zhu, D. L. Yin, S. B. Liu, J. Phys. Chem. C, 2010, **114**, 7196.

5. T. Matsuzawa, Y. Aoki, N. Takeuchi, Y. Murayama, J. Electrochem. Soc., 1996, **143**, 2670.

6. K. Van den Eeckhout, P. F. Smet, D. Poelman, Mater., 2010, **3**, 2536.

7. T. Aitasalo, Jorma Hölsä, H. Jungner, M. Lastusaari, J. Niittykoski, J. Lumin., 2001, **94–95**, 59.

8. P. Dorenbos, J. Electrochem. Soc., 2005, **152**, H107.

9. Q. H. Zhang, J. Wang, Appl. Phys. A, 2012, **108**, 943.

10. M. M. Shang, G. G. Li, D. M. Yang, X. J. Kang, C. Peng, J. Lin, Dalton Trans., 2012, **41**, 8861.

11. C. Bertail, S. Maron, V. Buissette, T. L. Mercier, T. Gacoin, J.-P. Boilot, Chem. Mater., 2011, **23**, 2961.

12. G. B. Che, C. B. Liu, X. Y. Li, Z. L. Xu, Y. Liu, H.Wang, J. Phys. Chem. Solids, 2008, **69**, 2091.

13. J. Y. Kuang, Y. L. Liu, B. F. Lei, J. Lumin., 2006, **118**, 33.

14. W. D. Partlow, D. W. Feldman, J. Lumin., 1973, **6**, 11.

15. J. Rodriguez-Carvajal, Reference Guide for the Computer Program FullProf. Laboratoire LeÂon Brillouin, CEA-CNRS, Saclay, France, 1996.

16. E. Plattner, H. Völlenke, A. Wittmann, Monatsh. Chem., 1976, **107**, 921.

17. L. Sebastian, R. S. Jayashree, J. Gopalakrishnan, J. Mater. Chem., 2003, **13**, 1400.

18. Z. S. Liu, X. P. Jing, L. X. Wang, J. Electrochem. Soc., 2007, **154**, H500.

19. M. M. Shang, G. G. Li, D. M. Yang, X. J. Kang, C. Peng, Z. Y. Cheng, J. Lin, Dalton Trans., 2011, **40**, 9379.

20. K. Uheda, T. Maruyama, H. Takizawa, T. Endo, J. Alloys Compd., 1997, **262-263**, 60.

21. S. Thomast, M. Banerjeet, P. B. Vidyasagart, A. D. Shaligramz, Meas. Scl. Technol., 1995, **6**, 554.

22. Y. H. Jin, Y. H. Hu, L. Chen, X. J. Wang, Z. F. Mou, G. F. Ju, F. Liang, Mater. Sci. Eng., B, 2013, **78**, 1205.

23. X. H. Xu, Y. H. Wang, W. Zeng, Y. Gong, B. T. Liu, J. Am. Ceram. Soc., 2011, **94**, 3632.

24. Y. L. Liu, B. F. Lei, C. S. Shi, Chem. Mater., 2005, **17**, 2108.

25. K. Van den Eeckhout, A. J. J. Bos, D. Poelman, P. F. Smet, Phys. Rev. B, 2013, **87**, 045126.

Figure captions

Fig.1 XRD patterns of some representative samples LZGO:tMn (t=0, 0.0025, 0.01 and 0.02).

Fig.2 Rietveld refinement of powder XRD profiles all obtained samples LZGO:tMn ((a)-(f) correspond to t=0, 0.0025, 0.005, 0.01, 0.015 and 0.02, respcetively).

Fig.3 (a) Excitation spectra of LZGO (λ_{em}=393 nm) and LZGO:Mn^{2+} (λ_{em}=530 nm) along with the emission spectra of LZGO (λ_{ex}=245 nm) and LZGO:Mn^{2+} (λ_{ex}=266 nm); (b) The amplified excitation spectrum of LZGO in the wavelength range from 350 to 500 nm; (c) The amplified emission spectrum of LZGO:Mn^{2+} between 300 and 450 nm.

Fig.4 The afterglow spectra of all obtained samples after the removal of 254 nm excitation. Insets: the photos of LZGO and LZGO:tMn samples under sunlight, under the irradiation by 254 nm and after the removal of excitation in dark, respectively.

Fig.5 Afterglow decay curves of samples LZGO:tMn (t=0, 0.0025, 0.005, 0.01, 0.015 and 0.02) from 0 to 1000 s.

Fig.6 TL curves of samples LZGO:tMn (t=0, 0.0025, 0.005, 0.01, 0.015 and 0.02).

Fig.7 The schematic model of phosphorescence mechanism in long afterglow phosphors of LZGO and LZGO:Mn.

Table 1 (a) Crystallographic data and structure parameters of samples LZGO:tMn^{2+} (t=0, 0.0025, 0.005, 0.01, 0.015 and 0.02) and (b) the goodness of fitting parameters.

(a)

Parameters	Samples	Zn	Ge	Li1	Li2	O1	O2	O3	O4	Mn
x	t=0	0.251	0	0.493	0.724	0.469	0.271	0.997	0.250	—
	t=0.0025	0.251	0	0.460	0.729	0.467	0.271	0.997	0.242	0.251
	t=0.005	0.253	0	0.504	0.729	0.473	0.285	0.997	0.245	0.253
	t=0.01	0.252	0	0.480	0.737	0.467	0.271	0.997	0.244	0.252
	t=0.015	0.252	0	0.449	0.739	0.450	0.268	0.997	0.246	0.252
	t=0.02	0.252	0	0.479	0.731	0.469	0.268	0.997	0.243	0.252
y	t=0	0.333	0.165	0.190	0.364	0.160	0.669	0.161	0.313	—
	t=0.0025	0.332	0.168	0.188	0.349	0.151	0.668	0.160	0.312	0.332
	t=0.005	0.330	0.170	0.192	0.365	0.125	0.651	0.158	0.310	0.330
	t=0.01	0.331	0.167	0.200	0.358	0.143	0.672	0.170	0.310	0.331
	t=0.015	0.331	0.168	0.202	0.345	0.135	0.672	0.164	0.319	0.331
	t=0.02	0.332	0.167	0.202	0.345	0.144	0.662	0.153	0.310	0.332
z	t=0	0.541	0.039	0.005	0.520	0.381	0.447	0.381	0.903	—
	t=0.0025	0.542	0.039	0.005	0.505	0.410	0.448	0.390	0.915	0.542
	t=0.005	0.541	0.039	0.005	0.511	0.396	0.456	0.404	0.894	0.541
	t=0.01	0.541	0.039	0.005	0.517	0.413	0.444	0.390	0.912	0.541
	t=0.015	0.542	0.039	0.005	0.512	0.415	0.440	0.393	0.913	0.542
	t=0.02	0.543	0.039	0.005	0.518	0.413	0.445	0.393	0.911	0.543
Occupancy factor	t=0	1.0	1.0	1.0	1.0	1.0	1.0	1.0	1.0	—
	t=0.0025	0.998	1.0	1.0	1.0	1.0	1.0	1.0	1.0	0.002
	t=0.005	0.995	1.0	1.0	1.0	1.0	1.0	1.0	1.0	0.005
	t=0.01	0.99	1.0	1.0	1.0	1.0	1.0	1.0	1.0	0.01
	t=0.015	0.985	1.0	1.0	1.0	1.0	1.0	1.0	1.0	0.015
	t=0.02	0.98	1.0	1.0	1.0	1.0	1.0	1.0	1.0	0.02
Unit cell parameters and the errors	t=0	a=6.363(2)Å, b=5.434(1)Å, c=5.033(1)Å, β=90.204(2)°								
	t=0.0025	a=6.363(1)Å, b=5.435(1)Å, c=5.033(1)Å, β=90.209(1)°								
	t=0.005	a=6.364(1)Å, b=5.435(2)Å, c=5.033(2)Å, β=90.207(2)°								
	t=0.01	a=6.364(1)Å, b=5.436(1)Å, c=5.033(1)Å, β=90.207(1)°								
	t=0.015	a=6.365(1)Å, b=5.435(1)Å, c=5.034(1)Å, β=90.204(1)°								
	t=0.02	a=6.366(1)Å, b=5.435(1)Å, c=5.034(1)Å, β=90.205(2)°								

(b)

	t=0	t=0.0025	t=0.005	t=0.01	t=0.015	t=0.02
R_P (%)	10.1	8.53	9.37	7.25	6.72	7.03
R_{WP} (%)	12.0	10.3	11.6	9.08	8.16	8.40
χ^2	2.58	1.75	2.09	1.57	1.21	1.16

Table 2 Decay times for two exponential components of LZGO:tMn^{2+} (t=0, 0.0025, 0.005, 0.01, 0.015 and 0.02) with different concentrations of Mn^{2+}.

Contents of Mn^{2+} (t)	τ_1(s)	I_1	$\tau_2(s)$	I_2
0	13	21321	257	3213
0.0025	46	149683	386	45954
0.005	34	94571	328	26584
0.01	18	34719	326	3739
0.015	18	13568	273	1737
0.02	14	4450	171	1165

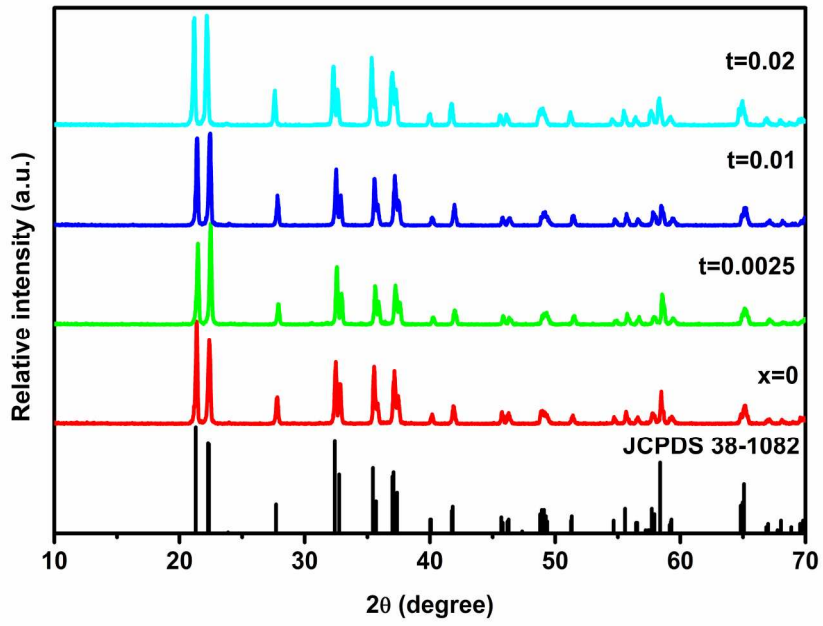

Fig.1 XRD patterns of some representative samples LZGO:tMn (t=0, 0.0025, 0.01 and 0.02).
201x141mm (300 x 300 DPI)

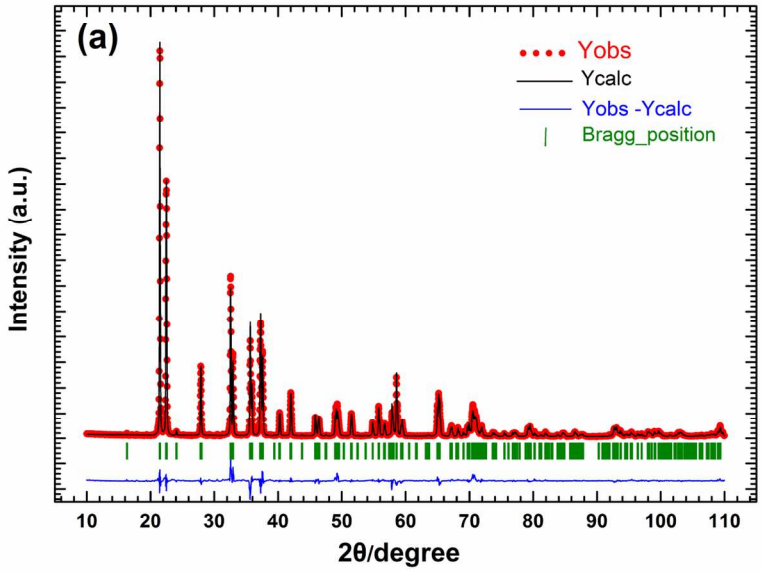

Fig.2 (a)
139x97mm (300 x 300 DPI)

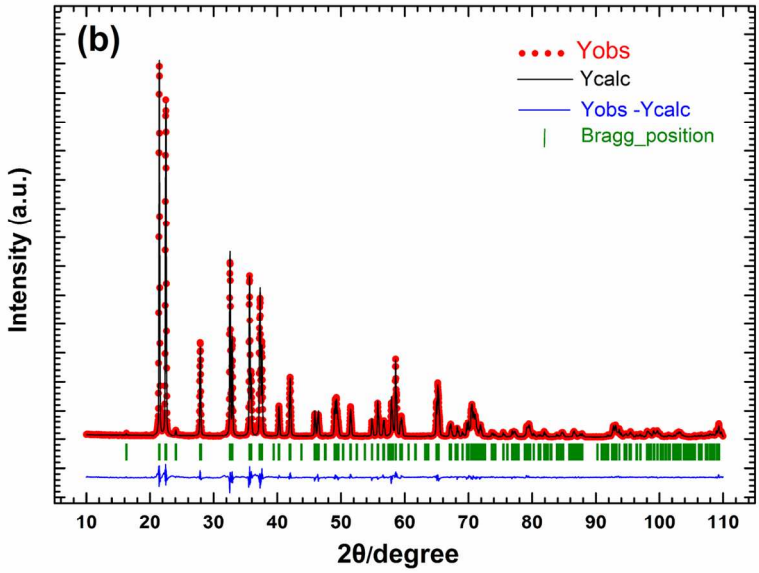

Fig.2 (b)
139x97mm (300 x 300 DPI)

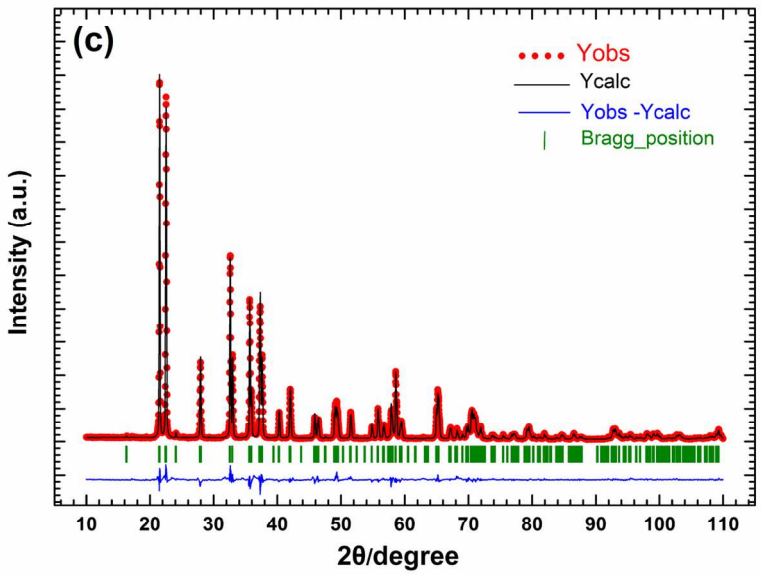

Fig.2 (c)
139x97mm (300 x 300 DPI)

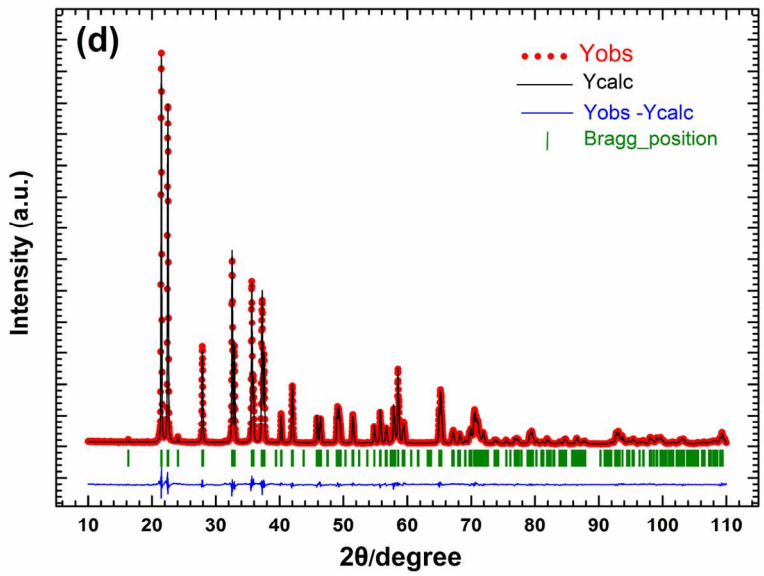

Fig.2 (d)
139x97mm (300 x 300 DPI)

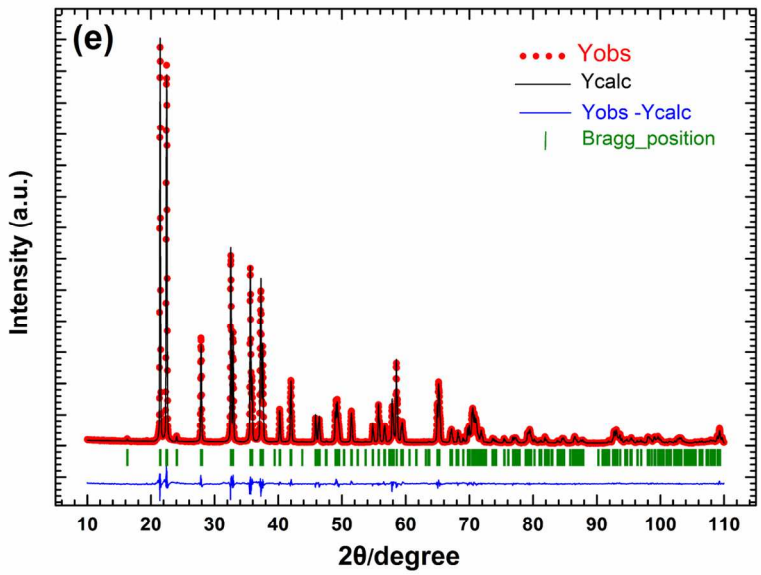

Fig.2 (e)
139x97mm (300 x 300 DPI)

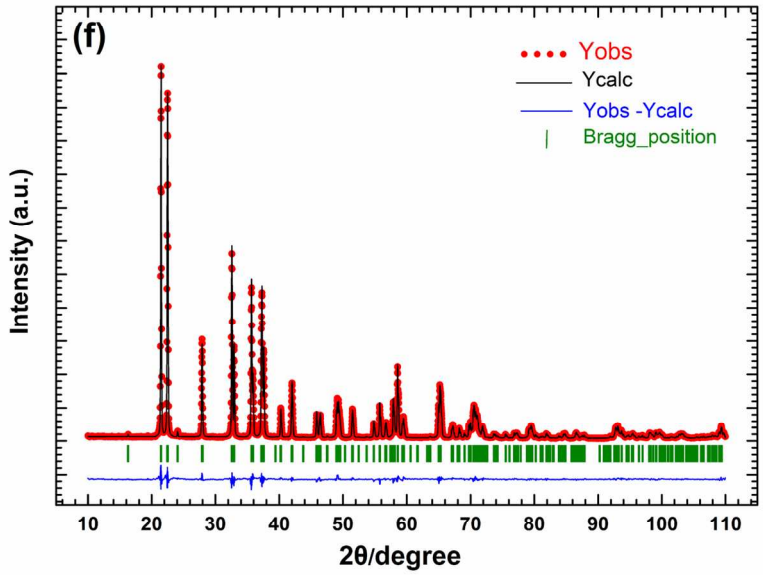

Fig.2 Rietveld refinement of powder XRD profiles all obtained samples LZGO:tMn ((a)-(f) correspond to t=0, 0.0025, 0.005, 0.01, 0.015 and 0.02, respcetively).
139x97mm (300 x 300 DPI)

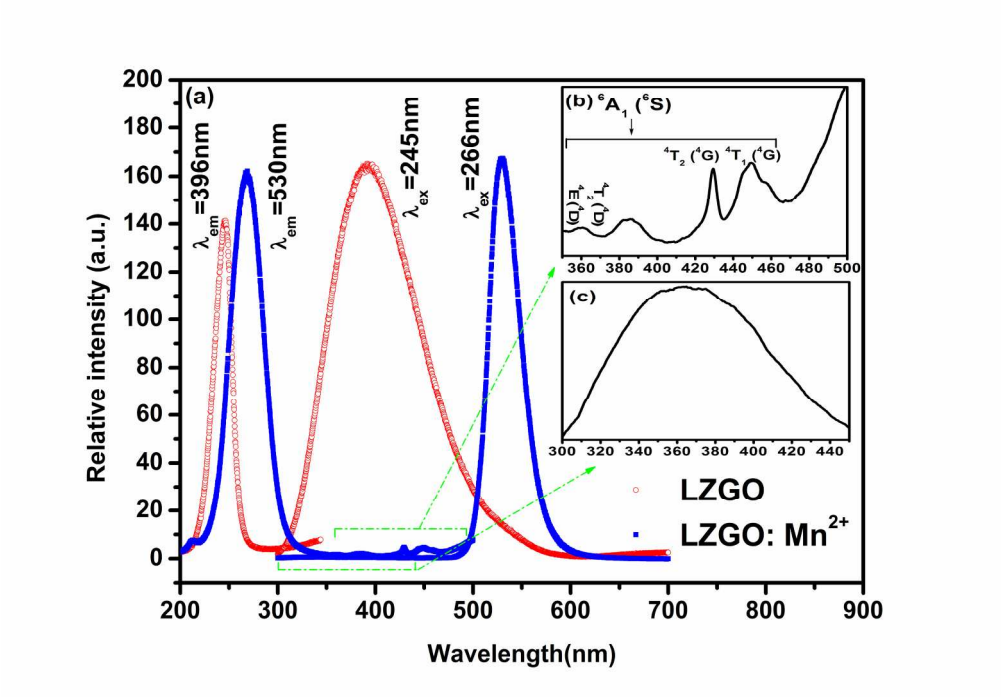

Fig.3 (a) Excitation spectra of LZGO (λ_{em}=393 nm) and LZGO:Mn^{2+} (λ_{em}=530 nm) along with the emission spectra of LZGO (λ_{ex}=245 nm) and LZGO:Mn^{2+} (λ_{ex}=266 nm); (b) The amplified excitation spectrum of LZGO in the wavelength range from 350 to 500 nm; (c) The amplified emission spectrum of LZGO:Mn^{2+} between 300 and 450 nm.
201x141mm (300 x 300 DPI)

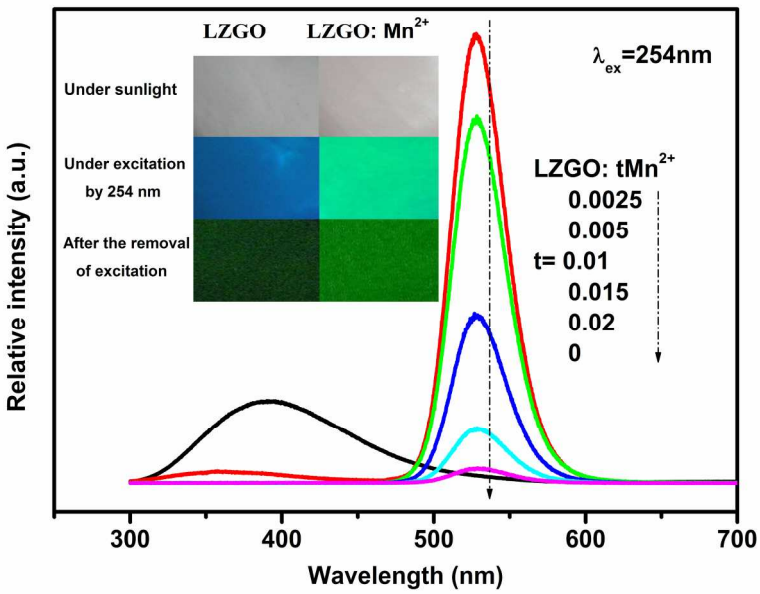

Fig.4 The afterglow spectra of all obtained samples after the removal of 254 nm excitation. Insets: the photos of LZGO and LZGO:tMn samples under sunlight, under the irradiation by 254 nm and after the removal of excitation in dark, respectively.
201x141mm (300 x 300 DPI)

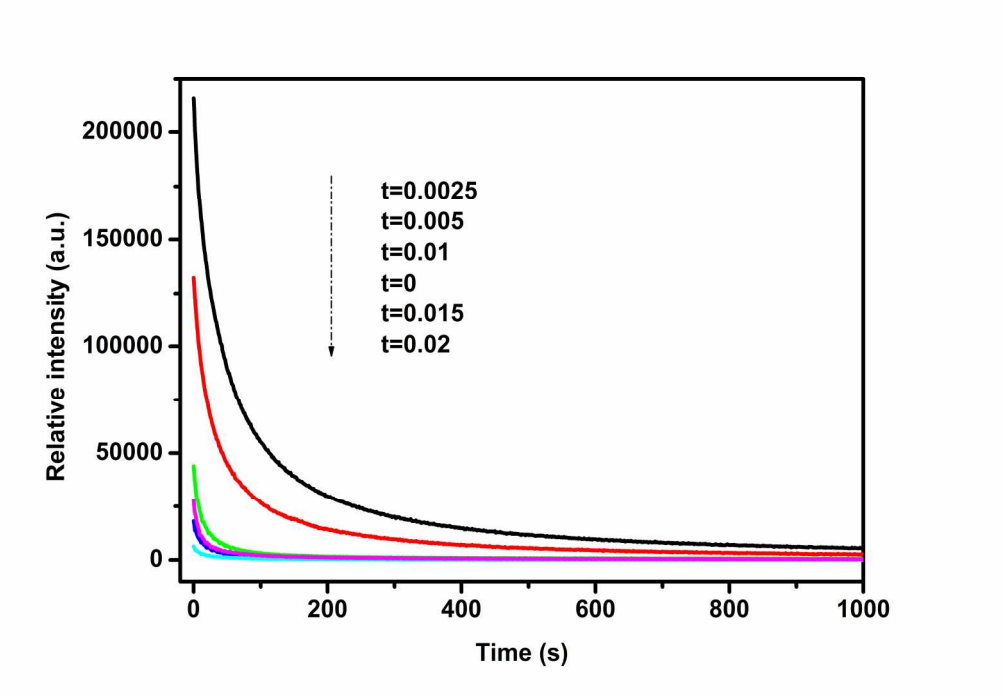

Fig.5 Afterglow decay curves of samples LZGO:tMn (t=0, 0.0025, 0.005, 0.01, 0.015 and 0.02) from 0 to 1000 s.
201x141mm (300 x 300 DPI)

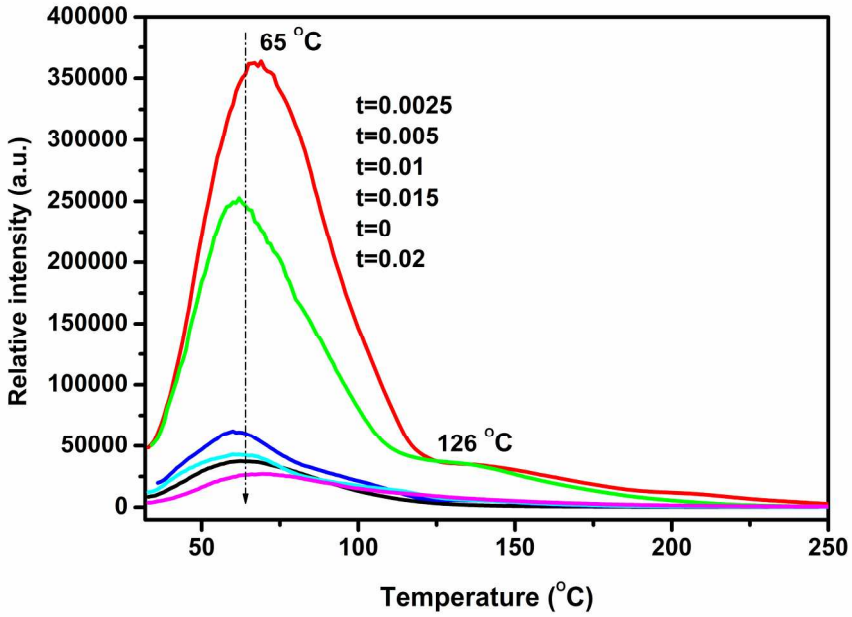

Fig.6 TL curves of samples LZGO:tMn (t=0, 0.0025, 0.005, 0.01, 0.015 and 0.02).
201x141mm (300 x 300 DPI)

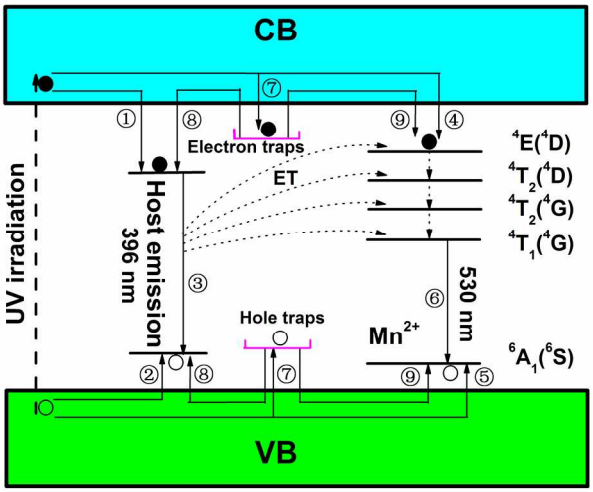

Fig.7 The schematic model of phosphorescence mechanism in long afterglow phosphors of LZGO and LZGO:Mn.

201x141mm (300 x 300 DPI)